Volume 6
Number 2
February 2026
Pages 121–240

Environmental Science
Atmospheres

rsc.li/esatmospheres

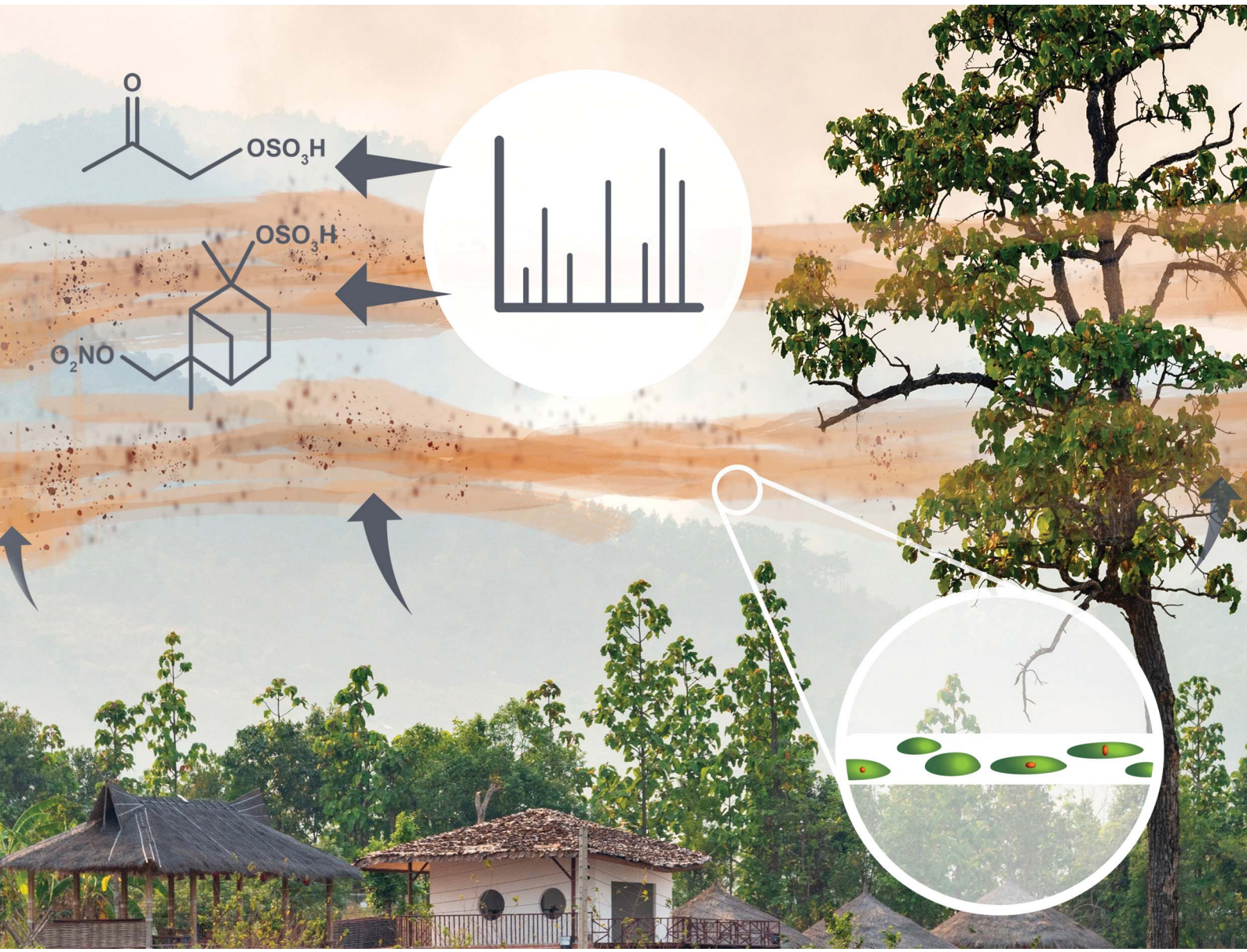

ISSN 2634-3606

ROYAL SOCIETY OF CHEMISTRY

PAPER
Swarup China *et al.*
Haze processing of atmospheric particles during wintertime in the Indo-Gangetic Plains

Environmental Science: Atmospheres

ROYAL SOCIETY OF CHEMISTRY

PAPER

View Article Online
View Journal | View Issue

Cite this: *Environ. Sci.: Atmos.*, 2026, **6**, 139

Haze processing of atmospheric particles during wintertime in the Indo-Gangetic Plains

Susan Mathai, †[ab] Amna Ijaz, ‡[ab] Tania Gautam,‡[a] Zezhen Cheng, [a] Nurun Nahar Lata, [a] Harsh Bhotika, [a] David Tseng,[a] Rosalie K. Chu,[a] Lynn Mazzoleni,[b] Claudio Mazzoleni [b] and Swarup China *[a]

Received 18th November 2025
Accepted 3rd January 2026

DOI: 10.1039/d5ea00150a

rsc.li/esatmospheres

The impacts of haze on visibility, air quality, and climate are not well quantified due to a lack of understanding of the evolution of the mixing state and phase state of atmospheric particles during haze processing. The variability of the mixing state of atmospheric particles contributes significantly to uncertainties associated with the estimated aerosol radiative forcing. We collected particle samples in January 2018 from the highly polluted Indo-Gangetic plain during hazy conditions to study haze-processed particles. Single particle analysis using multi-modal micro-spectroscopy techniques revealed an abundance (40–70% by number) of potassium-rich sulfate particles from biomass-burning influenced smoke. Tilted view imaging showed that most of the organic particles that had inorganic potassium and sulfate inclusions were liquid-like while those without inclusions were more semi-solid. High-resolution mass spectrometry analysis revealed a significant presence of organosulfates and nitroxy-organosulfates in the morning samples (24%) compared to the afternoon samples (9%), despite higher relative humidity in the afternoon. Overall, our results highlight the significant contribution of both organic and inorganic sulfate to the total particulate sulfur budget during haze processing in winter, when anthropogenic emissions such as household burning, agricultural burning, and vehicular emissions are major contributors to particle mass.

Environmental significance

Haze in the Indo-Gangetic Plain reduces visibility and harms the environment. Atmospheric particles play a critical role in forming haze, yet particle processing during hazy conditions remains poorly understood. This study investigates particle processing from single-particle to molecular-level during winter haze episodes originating from household fuel burning, agricultural residue burning, and vehicle emissions. Using advanced single-particle analysis and mass spectrometry techniques, this study reveals that winter haze contains abundant liquid-like particles enriched in potassium and sulfates, with compositions that vary by source and time of day. These variations influence how particles interact with sunlight and water vapor in the atmosphere. This study highlights the central role of both organic and inorganic emissions from everyday activities in driving winter haze formation.

1 Introduction

Haze, a suspension of particles in the atmosphere that scatters light,[1] reduces visibility to less than 10 km due to the high accumulation of fine aerosols.[2] Haze has adverse effects on human health, climate, and the environment.[3] Severe haze is a major concern all around the world such as in France,[4] China,[5] Mexico City,[6] India,[7] Bolivia in South America,[8] San Joaquin Valley in California,[8] and the Po Valley in Italy.[8] The northern parts of India and China often experience severe haze, typically during winter when particle concentrations are as high as several hundred μg m^{-3}.[9,10] This study focuses on the Indo-Gangetic Plain (IGP), which includes most of the northern regions of the Indian subcontinent (~21% of land area) and is one of the most populated and polluted regions in the world.[11] The area is polluted by wildfires and a wide range of anthropogenic activities such as biomass and fossil fuel burning, industries, transport, mining, agricultural, and urbanization.[11] The pollution can have contributions from the IGP region (West Bengal), which hosts a large number of coal mines, and iron and steel industries.[12] During winter, the estimated atmospheric particulate matter mass concentration ($PM_{2.5}$) in the city of Kolkata, situated in the IGP, is 100 μg m^{-3}, comparable to other highly polluted cities in India such as Delhi.[13] These high particle concentrations during winter lead to increase haze

[a]*Environmental Molecular Sciences Laboratory, Pacific Northwest National Laboratory, Richland, WA 99354, USA. E-mail: Swarup.China@pnnl.gov; Tel: +1 509 371-7329*

[b]*Michigan Technological University, Houghton, MI-49931, USA*

† Now at: NASA Langley Research Center, Hampton, Virginia 23666, United States; Oak Ridge Associated Universities, Oak Ridge, Tennessee 37830, United States.

‡ Now at: Atmospheric, Climate, and Earth Sciences Division, Pacific Northwest National Laboratory, Richland, WA 99352, United States.

occurrences, from 2003 to 2017, at a rate of about 2.6 days per year over IGP and about 1.7 days per year over central India.[14]

Since aerosols undergo multiphase reactions with high liquid water content, unraveling the chemical composition of aerosols during haze episodes is an active area of research. The highly acidic environment of the IGP region during winter due to the high concentration of sulfate aerosols leads to the formation of secondary organic aerosol (SOA), which impacts the air quality and visibility.[15] Under high relative humidity conditions during haze episodes, aerosol undergoes both physical (solid to liquid state) and chemical (formation of SOA *via* heterogeneous reactions such as SO_2 heterogeneous oxidation, N_2O_5 hydrolysis[16,17] *etc.*) transformations due to aqueous phase chemistry.[18] Enhanced formations of water-soluble secondary inorganic aerosols such as sulfates, nitrates, ammonium, and SOA are observed due to favorable meteorological conditions in this region such as low wind speed, frequent temperature inversions, high humidity, and shallow boundary layer.[15,19]

Most of the studies from the IGP region focused on the chemical composition of bulk aerosol samples collected during haze episodes, but there is only a limited number of studies[20–22] that report individual particles' composition and molecular composition of bulk organic aerosol. Both individual particles' composition and molecular composition of organic aerosol are critical to understanding the complexity of particles, their impact on heterogeneous chemistry, and cloud formation. Given the dense urbanization in the IGP, acidic sulfate (SO_4^{2-}) and nitrate (NO_3^-) are consistently produced *via* atmospheric oxidation of SO_2 (g) and NO_x emitted from anthropogenic activities such as vehicles' driving, coal/oil refining, and brick kiln production.[23] In particular, 2-methyltetrol diastereomers (2-MTSs) have been extensively observed in isoprene-enriched environments under significant anthropogenic influence in other part of the world, contributing up to 13% of the organic carbon in aerosols.[24–26] Coupled with IGP's unique topography including meteorological drivers, the regional diversity of emitted pollutants[27,28] makes the composition of particles more complex. Additionally, molecular characterization of organosulfates (OSs) remains challenging due to the complexity of the SOA with large number of species and instrumental challenges in distinguishing OSs from inorganic sulfates.[29]

Chemical composition of particles further influences the phase state of particles which refers to the aerosol physical characteristic of being solid, semi-solid, or liquid, and it can change depending on environmental conditions like relative humidity and temperature. The phase state of the aerosols impact the gas-particle diffusion rates and play a major role in heterogeneous reactions, particle growth, and cloud condensation nuclei concentrations,[30] thereby impacting the aerosol optical depth.[31] Ambient organic particles often contain inorganic constituents (*e.g.*, sulfate, sodium) can increase the hygroscopicity of the particles and, at elevated relative humidity, enhance the water uptake of aerosols. Because of this water uptake, organic particles mixed with inorganic components might change phase from solid to semi-solid or liquid. With increasing relative humidity, the viscosity of organic particles decreases and becomes liquid-like particles.[32] For example, OS are important SOA constituents derived from the oxidation of biogenic[33] (*e.g.*, α-pinene, isoprene) and anthropogenic[34] (*e.g.*, industrial emissions, biomass burning) volatile organic compounds. OS mixed with inorganics can influence the phase transition of ambient aerosols, for instance, by reducing the deliquescence RH of inorganic salts.[31] While particle phase state and volatility are critical for understanding SOA formation, growth, and their atmospheric lifetime, our understanding of how these properties change under haze conditions remains limited. Single-particle measurements combined with molecular-level characterization are essential for resolving the distribution of aerosol phase state and volatility. Hence, further field observations are needed to understand how haze processing alters the phase state, mixing state, and volatility of the particles and their potential impact on the atmospheric environment.[35]

In this study, we investigate the chemical composition of individual particles as well as the bulk molecular composition of organic aerosols from a highly polluted region in the IGP under hazy conditions during wintertime. We utilize multimodal chemical and morphological imaging techniques to probe the chemical composition and morphology of individual particles and high-resolution mass spectrometry to investigate the molecular composition of the bulk aerosol by studying the molecular formulae (MFs).[36–39] Combined chemical imaging and high-resolution mass spectrometry (HRMS) analysis allow us to investigate the phase state and volatility of the different particle types. The goal of this study is to advance our understanding of single-particle composition, morphology and molecular composition of bulk aerosols during haze processing by establishing their relationships with aerosol phase state and volatility.

2 Experimental methods

2.1 Sampling site and sample collection

This study was conducted on the eastern side of the IGP (23° 24′N, 87°02′E) in West Bengal, India. Samples were collected during the winter of 2018 between January 2 and January 10 using a four-stage Sioutas Cascade Impactor (SKC Inc.). Particles were collected on substrates placed on the D stage (50% cut-off aerodynamic size is 0.25 μm) and C stage (50% cut-off aerodynamic size is 0.5 μm). The substrate used to collect the particles were TEM grids (copper 400 mesh grids coated with Carbon Type-B and lacey films, Ted Pella) and silicon nitride substrates (Silson). This study analyzed a set of seven samples (a total of 14 samples) noted as S1, S2, S3, S4, S5, S6, and S7 and combined stage C and stage D for each sample. Furthermore, bulk aerosol samples were collected on Teflon filters during the morning and afternoon of January 09 (F5 and F7). The sampling days (Table S1) were found to be hazy with humidity ranging from 31% to 78%. According to the Hybrid Single-Particle Lagrangian Integrated Trajectory (HYSPLIT) analysis (Fig. S1) and meteorological data, the air masses arriving at the site during sample collection likely passed through regions with low-lying cloud or fog along the IGP. Hence it is likely that the

particles experienced fog processing. In addition to long-range transported aerosols, there could be influence from local sources such as biomass burning from fields, household use of fuels, and vehicular exhaust.

2.2 Micro-spectroscopy analysis of particles

The elemental composition and morphology of the particles in each sample were determined using computer-controlled scanning electron microscopy with energy-dispersive X-ray spectroscopy analysis (CCSEM/EDX).[40] The analysis was conducted using an environmental scanning electron microscope (Thermo Fisher, Quanta). The microscope uses an energy dispersive X-ray analysis (EDX) spectrometer with a Si(Li) detector with an active area of 10 mm^2 and an atmospheric thin window. The X-ray spectra acquired using the EDX detector provided the elemental composition of the particles in the samples. The CCSEM/EDX was operated with a beam current of 500 pA and an accelerating voltage of 20 kV. Based on the elemental composition obtained from CCSEM/EDX, particles were classified into eight groups, such as Na-rich, Na-rich sulfates, Si-rich sulfates, carbonaceous–sulfates, K-rich sulfates, carbonaceous particles, and dust (Fig. S2). Particle classification is provided in Fig. S3. Particles with physical diameters ranging from 0.15 to 4.0 μm were analyzed in this study. At least 1000 particles from each sample were analyzed. Overall, we analyzed 16 982 individual particles in this study.

We observed from the SEM and TEM tilted view (75°) images that there are particles with inclusions that could impact the phase state of the particles. Hence, we subdivided the organic particles into two categories: (a) particles with inclusion (mostly potassium and sulfate), and (b) particles without inclusion. Using tilted angle electron microscopy, the deformation of the particles upon impact on the substrate was determined by calculating the aspect ratio of the particles (calculated as the ratio of the width of the particle to its height as measured in tilted view imaging accounting for the specific tilt view angle).[41] Based on the aspect ratio boundaries from a previous study, particles were grouped as solid (AR = 0.76 to 1), semi-solid (AR between 0.54 and 0.76), and liquid (AR below 0.54).[22] The aspect ratios were calculated for each sample except for S3 and S6 for which images were unavailable because they were damaged after initial analysis. Tilted view images were also captured using transmission electron microscopy to see the particle inclusion.

Scanning transmission X-ray microscopy along with near-edge X-ray absorption fine structure spectroscopy (STXM/NEXAFS) was utilized to determine the mixing state and carbon functionalities.[42] The transmitted X-ray beam through the sample was acquired at different energies and converted to an optical density (OD). Based on the observed absorption peak the functional groups for different mixing states in the sample were identified. We acquired STXM maps at 11 different energies of the carbon K-edge ranging from 278 to 320 eV and carbon spectra were acquired by capturing a stack of images at 111 energies in the same range (278–320 eV).

2.3 High-resolution mass spectrometry analysis of organic aerosols

The molecular composition of the organic fraction of aerosol in the F5 and F7 samples was determined using a 12-T Bruker SolariX Fourier-transform ion cyclotron resonance (FTICR) mass spectrometer (Bruker Daltronics, Billerica MA). The experimental conditions were based on a previous study.[43] Briefly, organics were extracted by immersing aerosol-loaded substrate in an 80 : 20 methanol solution in water, followed by filtration through a 0.2 μm PTFE syringe filter to remove insoluble material. Mass spectra obtained from field blank samples were subtracted from the measured spectra during data analysis. Mass spectra were acquired from m/z 100–900 by infusing the samples at 3.0 μL min^{-1} into an electrospray source operated in the negative mode with a glass capillary temperature of 180 °C. The needle voltage was set at +4.4 kV. A total of 300 scans were acquired with an ion accumulation time of 0.03 s. Mass lists were assigned formulae (±3 ppm) using MFAssignR[44] within the following constraints: $C_cH_hO_oN_{0-3}S_{0-1}P_{0-1}{}^{13}C_{0-2}{}^{34}S_{0-1}$, where the numbers of C, H, and O atoms was unrestricted; $0 \leq O/C \leq 2.0$; $0.3 \leq H/C \leq 2.5$, and $-13 \leq DBE\text{-}O \leq 20$. Further details on data processing can be found elsewhere.[45,46]

3 Results and discussion

3.1 Size-resolved particle composition and particle classes

As most of the sampling events were characterized by hazy conditions, our discussion primarily focuses on these events. The particle composition across samples was dominated by K-rich sulfates, accounting for 40 to 70% of the total particles analyzed. However, in S3, and S6, K-rich sulfates dropped below 20% while carbonaceous sulfates increased to about 40–50%, indicating SOA formation.[47] Fig. 1 shows the size-resolved particle composition of each sample.

K-rich sulfate particles are dominant, followed by Si-rich sulfates, carbonaceous sulfates, and Na-rich sulfates, respectively (Fig. 1). In the larger size fractions (1–4 μm), Si-rich sulfates constituted approximately 20–40% of the particle composition. Si-rich sulfates could be formed from the hydrated Si-rich minerals reacting with SO_2 emitted from coal combustion or agricultural burning.[48]

The abundance of K and Si-rich sulfates suggests potential contributions from both biomass burning and farming activities[49] as a previous study attributed the presence of K and Si in carbonaceous aerosol to agricultural activities and burning practices.[50] These K-salt particles present in the fresh smoke plumes of biomass burning transform into K_2SO_4 as part of aging in the atmosphere.[51]

Na-rich sulfates are present in smaller fractions accounting for 10 to 20% of the total number of particles in each sample except for S6 (<10%). Na is mostly emitted from sea spray and fungal spores, along with anthropogenic sources such as refuse incineration, oil combustion, coal combustion, car exhaust, and industrial pollution.[52]

Dust particles formed another consistent fraction (15–20%) in samples S1, S2, S3, S4, S6, and S7. S5 stood out, with dust

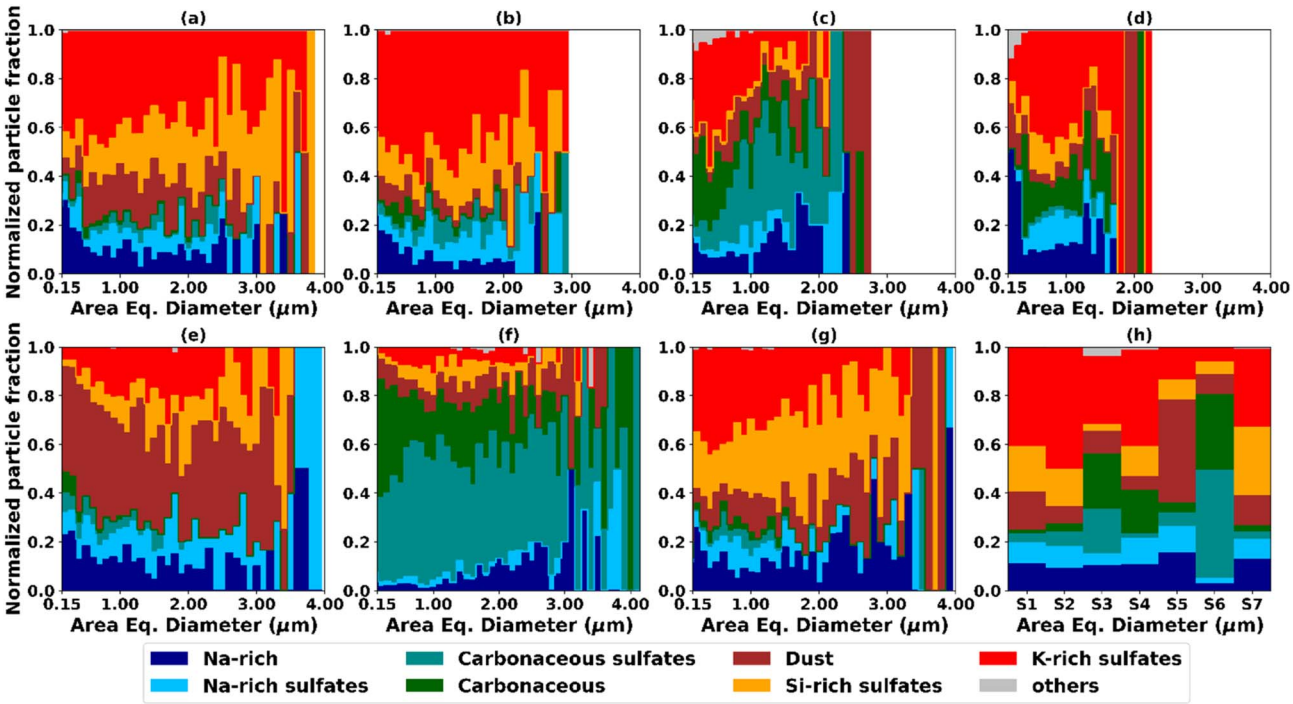

Fig. 1 Normalized particle number fraction for each particle class with respect to the area equivalent diameter for (a) 7:00 AM, 02 Jan, 2018 (S1); (b) 10:00 AM, 05 Jan, 2018 (S2); (c) 9:30 AM, 07 Jan, 2018 (S3); (d) 2:00 PM, 07 Jan, 2018 (S4); (e) 10:00 AM, 08 Jan, 2018 (S5); (f) 7:00 AM, 09 Jan, 2018 (S6); (g) 8:00 AM, 10 Jan, 2018 (S7), (h) a summary plot showing particle fractions averaged over all diameters. The total number of particles analyzed for S1, S2, S3, S4, S5 S6, and S7 are 2183, 2417, 1105, 2348 2534, 4958, and 1966 respectively.

comprising ~40% of the particle population and carbonaceous material dropping below 10% (Fig. 1). The dust in S5 was predominantly Si-rich or Fe-rich, potentially originating from fly ash or other combustion derived particulates. A previous study shows that in East Asia, fly ash and Fe-rich mineral dust are prevalent especially during aeolian dust events and have important radiative implication due to their strong light-absorbing properties.[53] Dust particles are frequently coated with organic material that may be present in a liquid phase, consistent with previous studies that identified aqueous-phase SOA coatings on aged dust particles.[54]

The overall high sulfate content in the particles is consistent with previous studies[55,56] that reported enhancement in sulfur during hazy days. For instance, an enhancement ratio (defined as the mean concentrations during haze divided by those during clean days) of 5.4 was observed for sulfates over North China.[55] In the IGP region, anthropogenic activities (*e.g.*, coal and oil burning, thermal power generation, road transport, commercial or residential burning, *etc.*) release SO_2 into the atmosphere.[57] Sulfate formation can be very common under hazy conditions through several pathways. For example, sulfur oxidation in the aqueous phase by hydrogen peroxide and ozone occurs much more rapidly than gas-phase oxidation by OH radicals.[58] Metal-catalyzed oxidation is another pathway to sulfate formation during haze events. For example, droplets containing dissolved Mn^{2+} absorb SO_2 at the surface of aerosol to form sulfates.[59] Another possible mechanism is the reaction of SO_2 emitted from coal combustion with the wet layer of adsorbed water vapor on non-carbonaceous particles, which eventually forms H_2SO_4.[60] This could lead to the formation of different non-carbonaceous sulfates observed in our samples. For instance, Na-rich particles could react with particulate H_2SO_4 to form Na-rich sulfates.[61]

3.2 Sulfate formation during haze

Since the previous section established the dominance of K-rich sulfates across the samples, this section further investigates their formation source and interactions with organic and sulfur-containing compounds. By studying the formation pathways of sulfate aerosols and their chemical composition, we aim to better understand the contribution of various sources, such as agricultural burning and other anthropogenic activities, to the IGP haze.[62,63] Particular attention is given to the formation of OS and nitroxy-OS, which are key components in haze episodes. Therefore, we investigated the sulfate formation pathways to understand the contribution of different sources. In a study by Li *et al.*, haze was classified into two types depending on the humidity and source.[51] Type 1 haze was formed from aerosols emitted from agricultural biomass burning and had particles larger than type 2 haze, which was formed from other anthropogenic sources, such as industrial pollution, transportation, and cooking. Weight percentage analysis indicated that haze formed due to agricultural burning showed a higher percentage of K with respect to S than what was present in laboratory-generated potassium sulfates; this is because of the abundance of KCl particles in fresh plumes of biomass burning.

Similarly, we also plotted the weight percentage of K against that of S for particles that were classified as potassium sulfate. In line with the study by Li *et al.*,[51] anthropogenic pollution can be a potential source of haze formation in the IGP (Fig. 2) with a high fraction of S.

Typically K is emitted as potassium chloride (KCl) into the atmosphere from fresh biomass-burning plumes and undergoes heterogeneous reactions to form potassium sulfates and nitrates.[64] EDX mapping of sampled particles shows that K and S are concentrated in small regions of the particles surrounded by carbon, oxygen, and nitrogen (Fig. S4). In line with this, 12-T FT-ICR MS presented formulae corresponding to well-known primary markers of wood combustion, including levoglucosan ($C_6H_{10}O_5$), acetosyringone ($C_{10}H_{12}O_4$), and sinapyl alcohol ($C_{11}H_{14}O_4$), in both samples, while others, such as coniferaldehyde ($C_{10}H_{10}O_3$), vanillin ($C_8H_8O_3$), acetovanillone ($C_9H_{10}O_3$), propiovanillone ($C_{10}H_{12}O_3$), methoxy eugenol ($C_{11}H_{14}O_3$), and nitrocatechol ($C_6H_5NO_4$) were found only in morning aerosol. Additionally, the chemical composition of sulfur-containing compounds, particularly OSs and nitroxy-OS, was explored with, considering that they are commonly found in severe haze episodes, where they usually originate from anthropogenic precursors.[65] The high abundance of these compounds is strongly indicative of aqueous-phase processing,[66] where gas-phase SO_2 and NO_x from anthropogenic sources are converted into acidic SO_4^{2-} and NO_3^- within haze droplets. These compounds' formation is facilitated by the acidic,[23] high humidity, haze conditions characteristic of the IGP.[67] Key formation pathways include the acid-catalysed ring-opening of VOC oxidation products, such as epoxides, aldehydes, and diverse multifunctional intermediates, which is a well-known mechanism for OS and nitroxy-OS formation in haze and fog.[68,69] Fig. 3 shows van Krevelen plots for the organic compounds characterized in the morning (F5) and afternoon (F7) samples, and the corresponding mass spectra are shown in Fig. S5. The morning sample presented much more molecular complexity (n = 5624 formulae) compared to the afternoon aerosol (n = 1637 formulae), which likely results from a combination of general and localized factors, such as accumulation of pollutants in a shallower nighttime boundary layer, enhanced aqueous-phase chemistry in the morning hazy conditions noted at the sampling location, lower temperatures in the morning that favour partitioning into the particle phase, as well as potentially unique anthropogenic morning-specific source activities in the Indo-Gangetic Plain. In line with this complexity, the morning sample was rich in both OS and nitroxy-OS, which constituted 24% of the total formulae assigned, but <10% of the total formulae in the afternoon aerosol. Nitroxy-OS compounds were not detected in the afternoon samples, whereas they constituted 10% of total molecular formulae in the morning sample (Fig. 3). Interestingly, the average relative humidity was significantly higher in the afternoon (78%) compared to the morning (43%), suggesting that relative humidity may not be the primary factor responsible for the presence of nitroxy-OS compounds in morning samples.

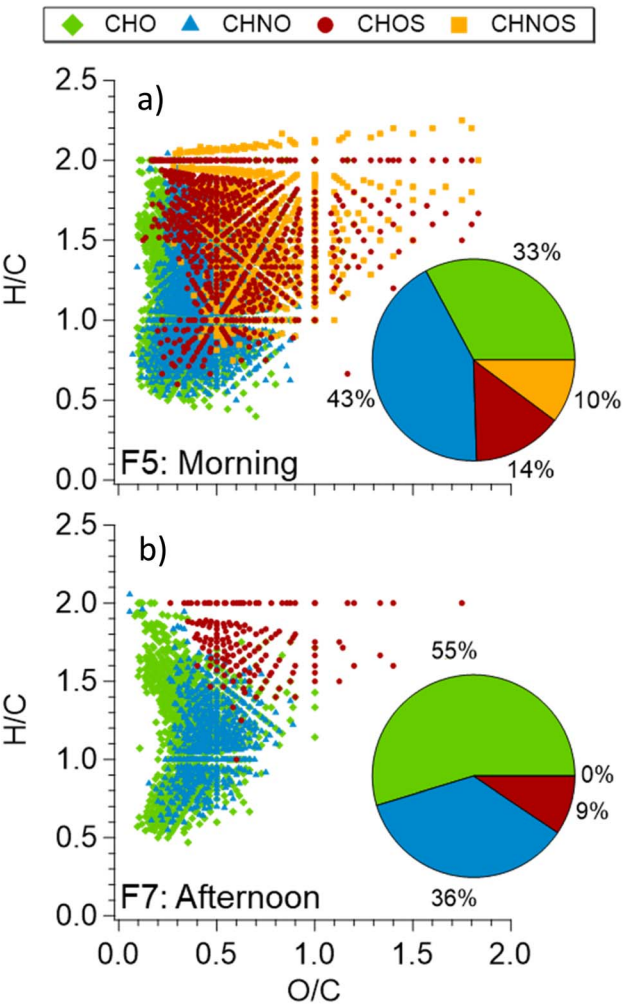

Fig. 3 Van Krevelen diagrams for molecular fractions in each sampling period (a) F5: morning and (b) F7: afternoon. The inset pie charts show the distribution of molecular formulae unique to the sampling period (morning *vs.* afternoon). The marker color indicates the class of identified molecular formulae.

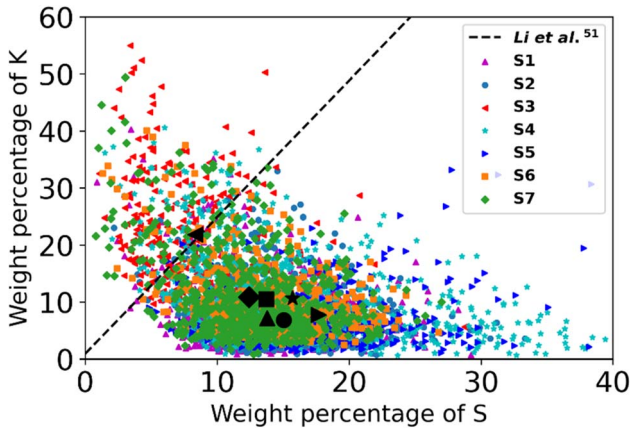

Fig. 2 Weight percentage of potassium with respect to that of sulfur for particles in the K-rich sulfate class. The dashed line represents the weight percentage of K and S for laboratory-generated K_2SO_4 from Li *et al.*[51] The black symbols represent the mean value for each sample.

Instead, the elevated levels of nitroxy-OS compounds in the morning may be attributed to overnight NO_3 radical chemistry, which could explain the overall higher abundance of CHNO compounds in morning samples compared to those collected in the afternoon. CHNO and CHNOS compounds have been reported as prevalent nighttime components that contributed more than 30% of the total light absorption by brown carbon during wintertime pollution in China.[70] Some specific examples of such compounds (or isobaric species) that have previously been observed during haze conditions in winter across urban China are presented in Table S3.[39,65,66,71,72]

A few of the identified OS and nitroxy-OS had noticeable trends. In particular, $C_9H_{15}O_7S^-$ had the highest intensity in both F5 and F7, and it has been previously observed in ambient cloud/fog water and free tropospheric biomass burning organic aerosol[72–75] (Table S3). In the work of Cai *et al.*,[39] O_7S species were found to be dominant in summertime, while Bryant *et al.*[76] showed an 8-fold enhancement in O_7S during wintertime. Since O_7S is predominantly found in the morning in our study, along with other OSs, it could have originated from the photochemical oxidation of common VOC precursors, such as monoterpenes[39] (*e.g.*, limonene or isoprene). The nitroxy-OS were exclusively observed in the morning sample (*e.g.*, $C_{10}H_{18}NO_9S$–, $C_{10}H_{16}NO_9S$–, $C_{12}H_{22}NO_9S$–, and $C_{12}H_{22}NO_8S$–). The compound with the highest peak intensity was $C_{10}H_{16}NO_9S$–, which could be a monoterpene-derived secondary product[39] as observed previously in urban aerosols during wintertime, as well as in fog water samples.[76,77] Previously, two pathways have been described for the formation of CHNOS, involving the conversion of primary CHOS species or the reaction of non-sulfur organic compounds with high concentrations of SO_x.[78] The addition of S-containing functional group generally reduces the light-absorption of CHNOS,[79,80] likely due to sulfate groups being non-chromophoric that creates a hypochromic effect.[81,82] While the overall optical properties of aerosol in the IGP have been explored in the upcoming sections, the abundance of potentially light-absorbing *N*- and *S*-functionalized species in this region is interesting and needs further investigation to determine their origin and implications.

The predominance of OS and nitroxy-OS and their volatility distributions in the morning sample can be seen in Fig. S5. A large majority of the compounds were classified as extremely low-volatility compounds (ELVOC) in both samples (Fig. S6), indicating that S-containing species are likely in the condensed (solid or liquid) phase that could have been produced *via* oxidative atmospheric processing.[39]

3.3 Chemical imaging of particles

Carbon functionalities of particles were studied using STXM/NEXAFS for two samples (S2 and S7) out of the seven samples due to resource constraints. We selected samples S2 and S7 because they contain a significant number of particles from all the identified classes and presented a better probability of capturing different types of particles using STXM/NEXAFS. The STXM/NEXAFS analysis was used to understand the influence of the mixing of inorganic material with carbonaceous particles on their phase state. Each particle is assumed to be a mixture of organic carbon (OC), elemental carbon (EC), and inorganic component (In). Fig. 4 shows representative NEXAFS spectra and maps of particles with four particle types. The peak at 288.5 eV indicates the presence of the carboxylic functional group, which can contribute to water uptake and increase in the viscosity of the particles with less oxygenated precursors.[83] In sample S7, OCEC accounted for ~35% of the total particle fraction out of ~250 particles analyzed whereas, while it only accounted for 20% in sample S2 (Fig. 4). An abundance of alkene groups in the particles represents soot or other sp^2-rich particles emitted from fossil fuel or biomass combustion.[36,37] Moreover, sample S2 contained approximately 30% of particles with the OCInEC, whereas less than 20% of the particles in S7 contained OCInEC. Further SEM analyses were conducted to explain the phase state of the particles in different samples.

We also investigated the phase state of these samples based on STXM data. The total carbon absorption (TCA) from STXM depends on the path length that X-ray photons travel through the particle, and it is used to estimate the particle phase state.[41] The threshold values for TCA to classify the particles into solid, semi-solid, and liquid states were obtained from a previous study.[37] Fig. 5c shows that particles with inorganic mixing (OCInEC and OCIn) were mostly in the liquid state. OCIn and OCInEC accounted for more than half of the particle fraction (~55%) in S2, whereas they accounted for only ~35% of the total particle fraction in S7. Previous laboratory studies suggest that inorganics are hygroscopic, and when they are internally mixed with organics, they enhance the overall hygroscopicity of the particle.[42,43] Moreover, a few field studies also report a decrease in the viscosity of the particles due to the presence of inorganics.[43,44] For instance, a field study by Slade *et al.* (2019)[84] using the University of Houston Mobile Air Quality Laboratory reported a decrease in the viscosity of the particles due to higher sulfate fraction during daytime. Similarly, another study by Cheng *et al.* 2022 also observed high abundance of liquid particles associated with inorganic inclusions.[41] Hence, our observation is consistent with previous studies.

The tilted view images from TEM and SEM showed an abundance of liquid-like flat-shaped particles in all the samples. TEM images in Fig. 5 show that liquid particles have inorganic inclusions with irregular shapes, while solid particles do not. Hence, we classified the particles into two groups: with and without inclusion. More than 90% of the organics with solid inclusions had an AR of less than 0.3 (except for sample S4), suggesting that they were mostly liquid. Whereas particles without inclusions existed in all three phase states, with solid or semi-solid states representing 42%, 31%, 67%, 47%, and 62% of the particles from S1, S2, S4, S5, and S7 samples respectively. Even though most of the samples (S1, S2, S5, and S7) showed an abundance of low-viscosity particles, sample S4, collected in the afternoon in hazy conditions (highest RH, 63% compared to other samples), showed considerably higher solid and semi-solid particles as compared to other samples. A potential explanation for this observation could be that the source of the particles for S4 is different. For example, S4 might be

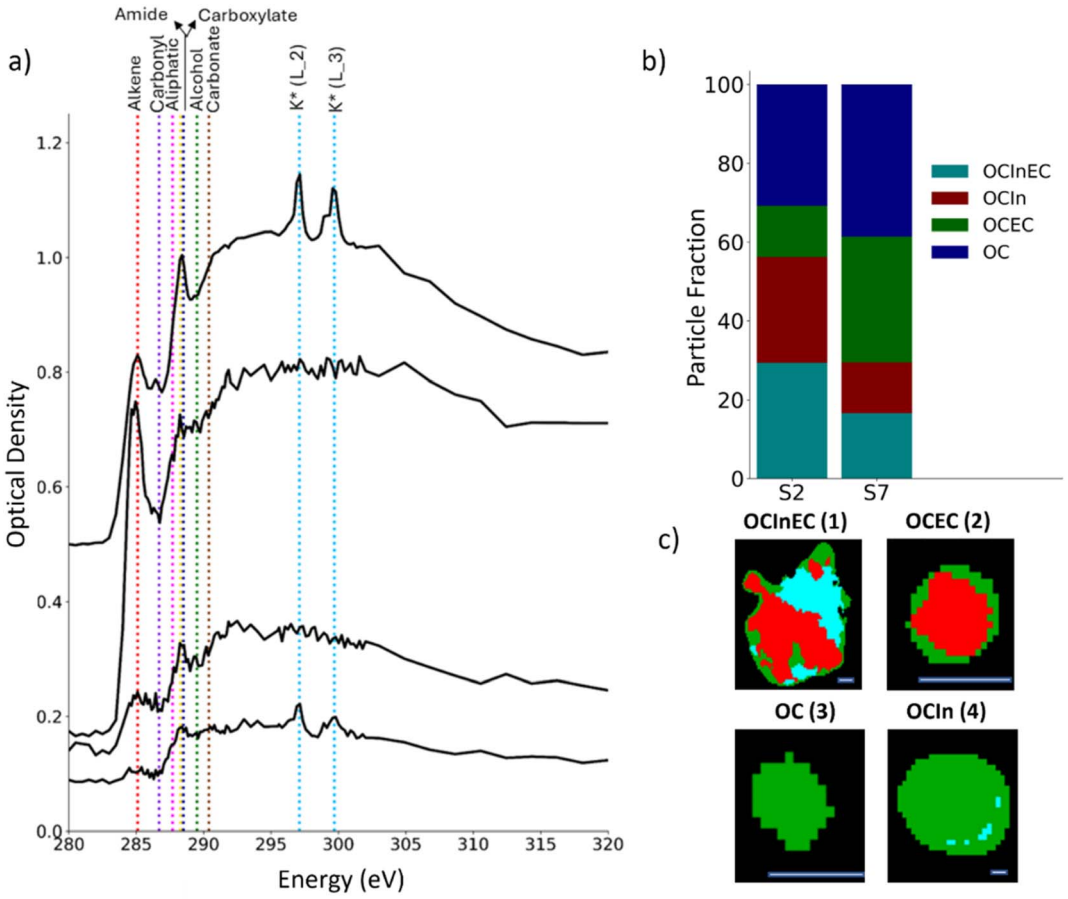

Fig. 4 (a) Representative STXM/NEXAFS spectra for different particle types. (b) Particle fraction of OC, OCIn, OCEC, and OCInEC for the S2 and S7 samples. (c) Carbon maps. The different colors in the carbon map represent organic carbon (green), organics and inorganics (blue), organics and elemental carbon (red), and a mixture of organic, elemental carbon and inorganics (teal). The dotted lines show peaks corresponding to the energies of different functional groups. The scale bar is 0.5 μm.

dominated by highly viscous tar ball-like particles as these particles were resistant to electron beam and spherical in shape.

Previous study also reported liquid-phase particles during heavy haze periods in urban atmospheres in China.[85] They suggested that elevated RH and increased inorganic fractions in particles enhance aerosol liquid water content, leading to the formation of liquid-phase particles. Similarly, another study found a predominance of semi-solid or solid particles during clean winter days with relative humidity below 30%, with a shift toward liquid-phase particles as relative humidity increased to 40–60%.[18]

4 Summary and environmental implications

This study aimed at understanding aerosol processing under haze conditions by determining the chemical composition, morphology, phase state, and volatility of particles collected during winter from the highly polluted region of the Indo-Gangetic Plain. The abundance of potassium sulfates in all samples suggests that biomass burning could be a major pollution source in the area.[87] Furthermore, we identified a diverse mixture of organonitrates, OSs, and nitroxy-OS, frequently present in urban aerosols. Nitroxy-OS are functionalized OS that are typically found as constituents of atmospheric aqueous media (*e.g.*, cloud, fog, and rainwater).[88,89] OS play a crucial role in the formation of SOA and enhance cloud condensation nuclei activity by affecting particle hygroscopicity.[90] The organonitrates in these aerosols can function as efficient light-absorbing brown carbon components, potentially influencing regional radiative balance and energy budget.[91,92]

Liquid-like particles with inorganic inclusions were found to be abundant in our samples. However, the afternoon sample (S4) showed particles with higher viscosity compared to the morning samples. Because the composition of low-viscosity particles changes more rapidly as they age due to faster diffusion of pollutants as compared to high-viscosity particles. Our findings suggest that morning particles might chemically evolve more rapidly than afternoon particles due to their low viscosity.[93] The observed dependence of particle phase state on inclusions and time of day underscores the complexity of haze processing, where factors beyond relative humidity, such as particle composition and mixing state govern physical properties. These results highlight the need for climate and chemical

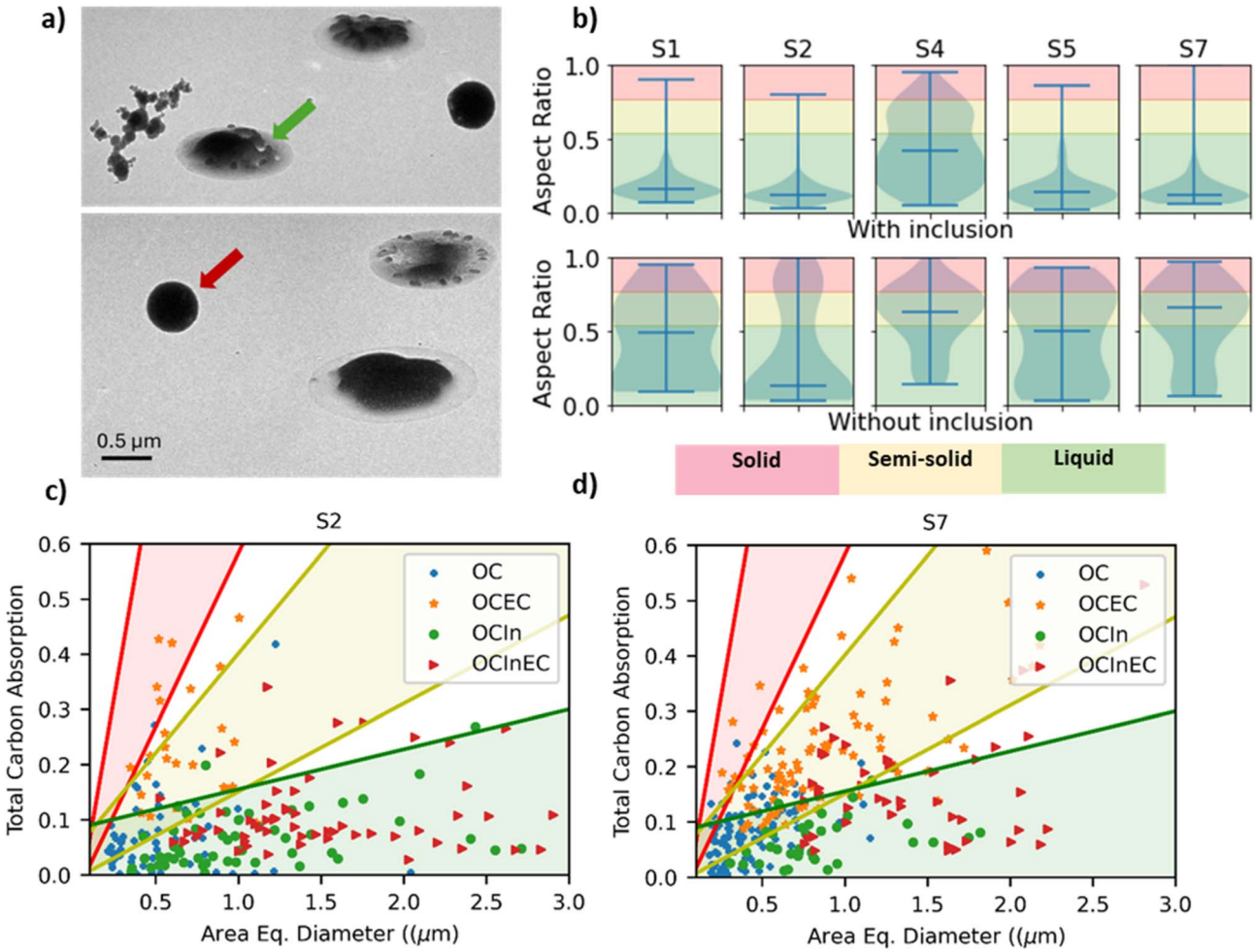

Fig. 5 (a) Tilted view TEM images show a liquid-like particle with inclusion (green arrow) (Sample S2) and a spherical particle without inclusion (red arrow) (Sample S4). Particles on S2 collected during daytime show liquid particles with inclusion and particles on S4 collected in the afternoon have spherical and solid particles. (b) Particles in each sample are grouped as particles with inclusions and particles without inclusions. The violin plots show the distribution of the aspect ratio values of the particles along with their medians and ranges. The thresholds used to classify the particles into liquid, semi-solid, and solid are from a previous study.[41] Total carbon absorption is plotted against area equivalent diameter for samples S2 (c) and S7 (d). Based on the thresholds used in a previous study, particles with different mixing states (OC, OCEC, OCIn, and OCInEC) are also classified into solid, semi-solid, and liquid particles.[86]

transport models to better represent source-specific aerosol composition, phase state, and viscosity under haze conditions. The presence of biomass-burning-derived OSs and organonitrates suggests that simplified model assumptions may misrepresent aerosol aging, cloud condensation nuclei activity, and radiative effects. From a policy perspective, reducing nighttime biomass burning and urban emissions could mitigate morning haze severity and provide co-benefits for air quality, visibility, and the regional environment in the IGP. While this study focuses on the IGP region, biomass burning is also a dominant source and wintertime haze is common in East Asia. Therefore, the observed particle phase state and volatility are likely to have similar implications across the broader East Asian region.

Author contributions

Conceptualization: S. M., C. M., and S. C. Formal analysis: S. M., A. I., T. G., Z. C., N. N. L., H. B., S. T., R. K. C., investigation: S. M., A. I., D. T., R. K. C., methodology: all authors. Resources: L. M., C. M., S. C., validation: S. M., A. I., C. M., S. C., visualization: S. M., A. I., H. B., writing – original draft: S. M. and A. I., writing – review and editing: all authors.

Conflicts of interest

The authors declare no competing financial interest.

Data availability

The data supporting this article has been included as part of the supplementary information (SI). Supplementary information:

sample collection and meteorological conditions; literature reported for single particle analysis and molecular formulae of organosulfates and nitroxy-organosulfates; satellite image and back trajectory analysis; particle analysis and classification; mass spectroscopy analysis. See DOI: https://doi.org/10.1039/d5ea00150a.

Acknowledgements

A portion of this research was performed on project awards (https://doi.org/10.46936/staf.proj.2020.51590/60000218 and https://doi.org/10.46936/lser.proj.2019.50795/60000103) and used resources at the Environmental Molecular Sciences Laboratory (EMSL) which is DOE Office of Science User Facilities. EMSL is sponsored by the Biological and Environmental Research program and operated under Contract No. DE-AC05-76RL01830. STXM/NEXAFS analysis at beamline 5.3.2 of the Advanced Light Source at Lawrence Berkeley National Laboratory is supported by the Director, Office of Science, Office of Basic Energy Sciences of the U.S. Department of Energy under Contract No. DE-AC02-05CH11231. S. M. acknowledges financial support from the Elizabeth and Richard Henes Center for Quantum Phenomena at Michigan Technological University.

References

1 Society A. M., Haze. https://glossary.ametsoc.org/wiki/Haze.
2 H. Fu and J. Chen, Formation, features and controlling strategies of severe haze-fog pollution in China, *Sci. Total Environ.*, 2017, **578**, 121–138.
3 A. J. Ding, X. Huang, W. Nie, J. N. Sun, V.-M. Kerminen, T. Petäjä, H. Su, Y. F. Cheng, X.-Q. Yang, M. H. Wang, X. G. Chi, J. P. Wang, A. Virkkula, W. D. Guo, J. Yuan, S. Y. Wang, R. J. Zhang, Y. F. Wu, Y. Song, T. Zhu, S. Zilitinkevich, M. Kulmala and C. B. Fu, Enhanced haze pollution by black carbon in megacities in China, *Geophys. Res. Lett.*, 2016, **43**(6), 2873–2879.
4 A. Fortems-Cheiney, G. Dufour, L. Hamaoui-Laguel, G. Foret, G. Siour, M. Van Damme, F. Meleux, P.-F. Coheur, C. Clerbaux, L. Clarisse, O. Favez, M. Wallasch and M. Beekmann, Unaccounted variability in NH3 agricultural sources detected by IASI contributing to European spring haze episode, *Geophys. Res. Lett.*, 2016, **43**(10), 5475–5482.
5 S. Guo, M. Hu, M. L. Zamora, J. Peng, D. Shang, J. Zheng, Z. Du, Z. Wu, M. Shao, L. Zeng, M. J. Molina and R. Zhang, Elucidating severe urban haze formation in China, *Proc. Natl. Acad. Sci. U. S. A.*, 2014, **111**(49), 17373–17378.
6 L. T. Molina, E. Velasco, A. Retama and M. Zavala, Experience from integrated air quality management in the Mexico City Metropolitan Area and Singapore, *Atmosphere*, 2019, **10**(9), 512.
7 D. Mishra, P. Goyal and A. Upadhyay, Artificial intelligence based approach to forecast PM2.5 during haze episodes: A case study of Delhi, India, *Atmos. Environ.*, 2015, **102**, 239–248.
8 R. B. Husar, J. D. Husar and L. Martin, Distribution of continental surface aerosol extinction based on visual range data, *Atmos. Environ.*, 2000, **34**(29), 5067–5078.
9 Z. An, R.-J. Huang, R. Zhang, X. Tie, G. Li, J. Cao, W. Zhou, Z. Shi, Y. Han, Z. Gu and Y. Ji, Severe haze in northern China: A synergy of anthropogenic emissions and atmospheric processes, *Proc. Natl. Acad. Sci. U. S. A.*, 2019, **116**(18), 8657–8666.
10 S. Kumari, N. Verma, A. Lakhani and K. M. Kumari, Severe haze events in the Indo-Gangetic Plain during post-monsoon: Synergetic effect of synoptic meteorology and crop residue burning emission, *Sci. Total Environ.*, 2021, **768**, 145479.
11 P. Chen, S. Kang, L. Tripathee, A. K. Panday, M. Rupakheti, D. Rupakheti, Q. Zhang, J. Guo, C. Li and T. Pu, Severe air pollution and characteristics of light-absorbing particles in a typical rural area of the Indo-Gangetic Plain, *Environ. Sci. Pollut. Res.*, 2020, **27**, 10617–10628.
12 V. S. Nair, K. K. Moorthy, D. P. Alappattu, P. K. Kunhikrishnan, S. George, P. R. Nair, S. S. Babu, B. Abish, S. K. Satheesh, S. N. Tripathi, K. Niranjan, B. L. Madhavan, V. Srikant, C. B. S. Dutt, K. V. S. Badarinath and R. R. Reddy, Wintertime aerosol characteristics over the Indo-Gangetic Plain (IGP): Impacts of local boundary layer processes and long-range transport, *J. Geophys. Res.: Atmos.*, 2007, **112**(D13), D13205.
13 D. Majumdar, R. Mondal, A. Periyasamy, N. Barman, S. Dey, S. Roy, P. Mandal, P. S. Rao and U. Sarkar, Characterization and sources of fine carbonaceous aerosol in winter over a megacity on Indo-Gangetic plain, *Urban Clim.*, 2021, **39**, 100964.
14 A. Thomas, C. Sarangi and V. P. Kanawade, Recent increase in winter hazy days over Central India and the Arabian Sea, *Sci. Rep.*, 2019, **9**(1), 17406.
15 K. Ram, M. M. Sarin and S. N. Tripathi, A 1 year record of carbonaceous aerosols from an urban site in the Indo-Gangetic Plain: Characterization, sources, and temporal variability, *J. Geophys. Res.: Atmos.*, 2010, **115**(D24), D24313.
16 Y. Cheng, G. Zheng, C. Wei, Q. Mu, B. Zheng, Z. Wang, M. Gao, Q. Zhang, K. He and G. Carmichael, Reactive nitrogen chemistry in aerosol water as a source of sulfate during haze events in China, *Sci. Adv.*, 2016, **2**(12), e1601530.
17 T. Liu, S. L. Clegg and J. P. Abbatt, Fast oxidation of sulfur dioxide by hydrogen peroxide in deliquesced aerosol particles, *Proc. Natl. Acad. Sci. U. S. A.*, 2020, **117**(3), 1354–1359.
18 X. Meng, Z. Wu, J. Chen, Y. Qiu, T. Zong, M. Song, J. Lee and M. Hu, Particle phase state and aerosol liquid water greatly impact secondary aerosol formation: insights into phase transition and its role in haze events, *Atmos. Chem. Phys.*, 2024, **24**(4), 2399–2414.
19 S. N. Behera and M. Sharma, Investigating the potential role of ammonia in ion chemistry of fine particulate matter formation for an urban environment, *Sci. Total Environ.*, 2010, **408**(17), 3569–3575.
20 N. Singh, T. Banerjee, V. Murari, K. Deboudt, M. F. Khan, R. S. Singh and M. T. Latif, Insights into size-segregated

particulate chemistry and sources in urban environment over central Indo-Gangetic Plain, *Chemosphere*, 2021, **263**, 128030.

21 A. Chakraborty, P. Rajeev, P. Rajput and T. Gupta, Water soluble organic aerosols in indo gangetic plain (IGP): Insights from aerosol mass spectrometry, *Sci. Total Environ.*, 2017, **599–600**, 1573–1582.

22 S. Izhar, T. Gupta, A. M. Qadri and A. K. Panday, Wintertime chemical characteristics of aerosol and their role in light extinction during clear and polluted days in rural Indo Gangetic plain, *Environ. Pollut.*, 2021, **282**, 117034.

23 S. Tiwari, P. K. Hopke, D. Thimmaiah, U. C. Dumka, A. K. Srivastava, D. S. Bisht, P. S. Rao, D. M. Chate, M. K. Srivastava and S. N. Tripathi, Nature and sources of ionic species in precipitation across the Indo-Gangetic Plains, India, *Aerosol Air Qual. Res.*, 2016, **16**(4), 943–957.

24 S. S. Petters, T. Cui, Z. Zhang, A. Gold, V. F. McNeill, J. D. Surratt and B. J. Turpin, Organosulfates from dark aqueous reactions of isoprene-derived epoxydiols under cloud and fog conditions: Kinetics, mechanism, and effect of reaction environment on regioselectivity of sulfate addition, *ACS Earth Space Chem.*, 2021, **5**(3), 474–486.

25 A. P. S. Hettiyadura, I. M. Al-Naiema, D. D. Hughes, T. Fang and E. A. Stone, Organosulfates in Atlanta, Georgia: anthropogenic influences on biogenic secondary organic aerosol formation, *Atmos. Chem. Phys.*, 2019, **19**(5), 3191–3206.

26 T. Cui, Z. Zeng, E. O. Dos Santos, Z. Zhang, Y. Chen, Y. Zhang, C. A. Rose, S. H. Budisulistiorini, L. B. Collins and W. M. Bodnar, Development of a hydrophilic interaction liquid chromatography (HILIC) method for the chemical characterization of water-soluble isoprene epoxydiol (IEPOX)-derived secondary organic aerosol, *Environ. Sci.: Processes Impacts*, 2018, **20**(11), 1524–1536.

27 V. Sinha, V. Kumar and C. Sarkar, Chemical composition of pre-monsoon air in the Indo-Gangetic Plain measured using a new air quality facility and PTR-MS: high surface ozone and strong influence of biomass burning, *Atmos. Chem. Phys.*, 2014, **14**(12), 5921–5941.

28 C. Mogno, P. I. Palmer, C. Knote, F. Yao and T. J. Wallington, Seasonal distribution and drivers of surface fine particulate matter and organic aerosol over the Indo-Gangetic Plain, *Atmos. Chem. Phys.*, 2021, **21**(14), 10881–10909.

29 A. L. Bondy, R. L. Craig, Z. Zhang, A. Gold, J. D. Surratt and A. P. Ault, Isoprene-derived organosulfates: Vibrational mode analysis by Raman spectroscopy, acidity-dependent spectral modes, and observation in individual atmospheric particles, *J. Phys. Chem. A*, 2018, **122**(1), 303–315.

30 W. Xu, C. Chen, Y. Qiu, Y. Li, Z. Zhang, E. Karnezi, S. N. Pandis, C. Xie, Z. Li and J. Sun, Organic aerosol volatility and viscosity in the North China Plain: contrast between summer and winter, *Atmos. Chem. Phys.*, 2021, **21**(7), 5463–5476.

31 A. D. Estillore, A. P. S. Hettiyadura, Z. Qin, E. Leckrone, B. Wombacher, T. Humphry, E. A. Stone and V. H. Grassian, Water Uptake and Hygroscopic Growth of Organosulfate Aerosol, *Environ. Sci. Technol.*, 2016, **50**(8), 4259–4268.

32 Y. Zhang, M. Sanchez, C. Douet, Y. Wang, A. Bateman, Z. Gong, M. Kuwata, L. Renbaum-Wolff, B. Sato and P. Liu, Changing shapes and implied viscosities of suspended submicron particles, *Atmos. Chem. Phys.*, 2015, **15**(14), 7819–7829.

33 K. Kristensen and M. Glasius, Organosulfates and oxidation products from biogenic hydrocarbons in fine aerosols from a forest in North West Europe during spring, *Atmos. Environ.*, 2011, **45**(27), 4546–4556.

34 Y. Wang, M. Hu, S. Guo, Y. Wang, J. Zheng, Y. Yang, W. Zhu, R. Tang, X. Li, Y. Liu, M. Le Breton, Z. Du, D. Shang, Y. Wu, Z. Wu, Y. Song, S. Lou, M. Hallquist and J. Yu, The secondary formation of organosulfates under interactions between biogenic emissions and anthropogenic pollutants in summer in Beijing, *Atmos. Chem. Phys.*, 2018, **18**(14), 10693–10713.

35 M. Shrivastava, C. D. Cappa, J. Fan, A. H. Goldstein, A. B. Guenther, J. L. Jimenez, C. Kuang, A. Laskin, S. T. Martin, N. L. Ng, T. Petaja, J. R. Pierce, P. J. Rasch, P. Roldin, J. H. Seinfeld, J. Shilling, J. N. Smith, J. A. Thornton, R. Volkamer, J. Wang, D. R. Worsnop, R. A. Zaveri, A. Zelenyuk and Q. Zhang, Recent advances in understanding secondary organic aerosol: Implications for global climate forcing, *Rev. Geophys.*, 2017, **55**(2), 509–559.

36 K. Gao and T. Zhu, Analytical methods for organosulfate detection in aerosol particles: current status and future perspectives, *Sci. Total Environ.*, 2021, **784**, 147244.

37 R. E. O'Brien, A. Laskin, J. Laskin, C. L. Rubitschun, J. D. Surratt and A. H. Goldstein, Molecular characterization of S-and N-containing organic constituents in ambient aerosols by negative ion mode high-resolution nanospray desorption electrospray ionization mass spectrometry: CalNex 2010 field study, *J. Geophys. Res.: Atmos.*, 2014, **119**(22), 12706–12720.

38 S. Tao, X. Lu, N. Levac, A. P. Bateman, T. B. Nguyen, D. L. Bones, S. A. Nizkorodov, J. Laskin, A. Laskin and X. Yang, Molecular characterization of organosulfates in organic aerosols from Shanghai and Los Angeles urban areas by nanospray-desorption electrospray ionization high-resolution mass spectrometry, *Environ. Sci. Technol.*, 2014, **48**(18), 10993–11001.

39 D. Cai, X. Wang, J. Chen and X. Li, Molecular characterization of organosulfates in highly polluted atmosphere using ultra-high-resolution mass spectrometry, *J. Geophys. Res.: Atmos.*, 2020, **125**(8), e2019JD032253.

40 A. L. Bondy, D. Bonanno, R. C. Moffet, B. Wang, A. Laskin and A. P. Ault, The diverse chemical mixing state of aerosol particles in the southeastern United States, *Atmos. Chem. Phys.*, 2018, **18**(16), 12595–12612.

41 Z. Cheng, N. Sharma, K.-P. Tseng, L. Kovarik and S. China, Direct observation and assessment of phase states of ambient and lab-generated sub-micron particles upon humidification, *RSC Adv.*, 2021, **11**(25), 15264–15272.

42 R. J. Hopkins, A. V. Tivanski, B. D. Marten and M. K. Gilles, Chemical bonding and structure of black carbon reference

materials and individual carbonaceous atmospheric aerosols, *J. Aerosol Sci.*, 2007, **38**(6), 573–591.

43 M. M. Tfaily, R. K. Chu, N. Tolić, K. M. Roscioli, C. R. Anderton, L. Paša-Tolić, E. W. Robinson and N. J. Hess, Advanced Solvent Based Methods for Molecular Characterization of Soil Organic Matter by High-Resolution Mass Spectrometry, *Anal. Chem.*, 2015, **87**(10), 5206–5215.

44 S. K. Schum, L. E. Brown and L. R. Mazzoleni, MFAssignR: Molecular formula assignment software for ultrahigh resolution mass spectrometry analysis of environmental complex mixtures, *Environ. Res.*, 2020, **191**, 110114.

45 G. W. Vandergrift, N. N. Lata, S. Mathai, A. Ijaz, Z. Cheng, M. Shrivastava, J. Zhang, A. S. M. Shawon, G. Kulkarni and L. R. Mazzoleni, Case study evaluation of size-resolved molecular composition and phase state of carbonaceous particles in wildfire influenced smoke from the Pacific Northwest, *Environ. Sci.: Atmos.*, 2023, **3**(9), 1251–1261.

46 A. Ijaz, W. Kew, S. China, S. K. Schum and L. R. Mazzoleni, Molecular characterization of organophosphorus compounds in wildfire smoke using 21-T Fourier transform-ion cyclotron resonance mass spectrometry, *Anal. Chem.*, 2022, **94**(42), 14537–14545.

47 G. He, J. Ma and H. He, Role of Carbonaceous Aerosols in Catalyzing Sulfate Formation, *ACS Catal.*, 2018, **8**(5), 3825–3832.

48 J. Xing, L. Shao, F. Chen, W. Wang and D. Zhang, Characteristics and aging of traffic-emitted particles with sulfate and organic compound formation in urban air, *Atmosphere*, 2022, **13**(4), 608.

49 V. Murari, M. Kumar, N. Singh, R. Singh and T. Banerjee, Particulate morphology and elemental characteristics: variability at middle Indo-Gangetic Plain, *J. Atmos. Chem.*, 2016, **73**, 165–179.

50 S. Chantara, D. Thepnuan, W. Wiriya, S. Prawan and Y. I. Tsai, Emissions of pollutant gases, fine particulate matters and their significant tracers from biomass burning in an open-system combustion chamber, *Chemosphere*, 2019, **224**, 407–416.

51 W. Li, L. Shao and P. Buseck, Haze types in Beijing and the influence of agricultural biomass burning, *Atmos. Chem. Phys.*, 2010, **10**(17), 8119–8130.

52 S. China, S. M. Burrows, B. Wang, T. H. Harder, J. Weis, M. Tanarhte, L. V. Rizzo, J. Brito, G. G. Cirino and P.-L. Ma, Fungal spores as a source of sodium salt particles in the Amazon basin, *Nat. Commun.*, 2018, **9**(1), 4793.

53 N. Moteki, K. Adachi, S. Ohata, A. Yoshida, T. Harigaya, M. Koike and Y. Kondo, Anthropogenic iron oxide aerosols enhance atmospheric heating, *Nat. Commun.*, 2017, **8**(1), 15329.

54 W. Li, A. Ito, G. Wang, M. Zhi, L. Xu, Q. Yuan, J. Zhang, L. Liu, F. Wu, A. Laskin, D. Zhang, X. Zhang, T. Zhu, J. Chen, N. Mihalopoulos, A. Bougiatioti, M. Kanakidou, G. Wang, H. Hu, Y. Zhao and Z. Shi, Aqueous-phase secondary organic aerosol formation on mineral dust, *Natl. Sci. Rev.*, 2025, **12**(7), nwaf221.

55 Y. Wang, Q. Zhang, J. Jiang, W. Zhou, B. Wang, K. He, F. Duan, Q. Zhang, S. Philip and Y. Xie, Enhanced sulfate formation during China's severe winter haze episode in January 2013 missing from current models, *J. Geophys. Res.: Atmos.*, 2014, **119**(17), 10425–10440.

56 G. Li, N. Bei, J. Cao, R. Huang, J. Wu, T. Feng, Y. Wang, S. Liu, Q. Zhang and X. Tie, A possible pathway for rapid growth of sulfate during haze days in China, *Atmos. Chem. Phys.*, 2017, **17**(5), 3301–3316.

57 C. Mallik and S. Lal, Seasonal characteristics of SO2, NO2, and CO emissions in and around the Indo-Gangetic Plain, *Environ. Monit. Assess.*, 2014, **186**(2), 1295–1310.

58 B. Ervens, Modeling the Processing of Aerosol and Trace Gases in Clouds and Fogs, *Chem. Rev.*, 2015, **115**(10), 4157–4198.

59 W. Wang, M. Liu, T. Wang, Y. Song, L. Zhou, J. Cao, J. Hu, G. Tang, Z. Chen and Z. Li, Sulfate formation is dominated by manganese-catalyzed oxidation of SO2 on aerosol surfaces during haze events, *Nat. Commun.*, 2021, **12**(1), 1993.

60 W. Wang, L. Shao, M. Guo, C. Hou, J. Xing and F. Wu, Physicochemical Properties of Individual Airborne Particles in Beijing during Pollution Periods, *Aerosol Air Qual. Res.*, 2017, **17**(12), 3209–3219.

61 X. Liu, P. Van Espen, F. Adams, J. Cafmeyer and W. Maenhaut, Biomass burning in southern Africa: Individual particle characterization of atmospheric aerosols and savanna fire samples, *J. Atmos. Chem.*, 2000, **36**, 135–155.

62 A. Bharti, S. Bhardwaj, A. Srivastava, S. Banerjee and S. Sonwani, *Investigating the Problem of Crop Residue Burning in an Indo-Gangetic Plain (IGP)—An Emerging Concern to Air Quality*, 2021.

63 T. Saud, R. Gautam, T. Mandal, R. Gadi, D. Singh, S. Sharma, M. Dahiya and M. Saxena, Emission estimates of organic and elemental carbon from household biomass fuel used over the Indo-Gangetic Plain (IGP), India, *Atmos. Environ.*, 2012, **61**, 212–220.

64 G. Engling, J. J. Lee, Y.-W. Tsai, S.-C. C. Lung, C. C.-K. Chou and C.-Y. Chan, Size-resolved anhydrosugar composition in smoke aerosol from controlled field burning of rice straw, *Aerosol Sci. Technol.*, 2009, **43**(7), 662–672.

65 Y. Han, X. Zhang, L. Li, Y. Lin, C. Zhu, N. Zhang, Q. Wang and J. Cao, Enhanced Production of Organosulfur Species during a Severe Winter Haze Episode in the Guanzhong Basin of Northwest China, *Environ. Sci. Technol.*, 2023, **57**(23), 8708–8718.

66 Y. Zheng, Q. Chen, X. Cheng, C. Mohr, J. Cai, W. Huang, M. Shrivastava, P. Ye, P. Fu, X. Shi, Y. Ge, K. Liao, R. Miao, X. Qiu, T. K. Koenig and S. Chen, Precursors and Pathways Leading to Enhanced Secondary Organic Aerosol Formation during Severe Haze Episodes, *Environ. Sci. Technol.*, 2021, **55**(23), 15680–15693.

67 K. Ram, M. Sarin, A. Sudheer and R. Rengarajan, Carbonaceous and secondary inorganic aerosols during wintertime fog and haze over urban sites in the Indo-Gangetic Plain, *Aerosol Air Qual. Res.*, 2012, **12**(3), 359–370.

68 M. Brüggemann, R. Xu, A. Tilgner, K. C. Kwong, A. Mutzel, H. Y. Poon, T. Otto, T. Schaefer, L. Poulain and

M. N. Chan, Organosulfates in ambient aerosol: state of knowledge and future research directions on formation, abundance, fate, and importance, *Environ. Sci. Technol.*, 2020, **54**(7), 3767–3782.

69 A. I. Darer, N. C. Cole-Filipiak, A. E. O'Connor and M. J. Elrod, Formation and stability of atmospherically relevant isoprene-derived organosulfates and organonitrates, *Environ. Sci. Technol.*, 2011, **45**(5), 1895–1902.

70 Y. Zeng, Z. Shen, S. Takahama, L. Zhang, T. Zhang, Y. Lei, Q. Zhang, H. Xu, Y. Ning, Y. Huang, J. Cao and H. Rudolf, Molecular Absorption and Evolution Mechanisms of PM2.5 Brown Carbon Revealed by Electrospray Ionization Fourier Transform–Ion Cyclotron Resonance Mass Spectrometry During a Severe Winter Pollution Episode in Xi'an, China, *Geophys. Res. Lett.*, 2020, **47**(10), e2020GL087977.

71 M. Glasius, D. Thomsen, K. Wang, L. S. Iversen, J. Duan and R.-J. Huang, Chemical characteristics and sources of organosulfates, organosulfonates, and carboxylic acids in aerosols in urban Xi'an, Northwest China, *Sci. Total Environ.*, 2022, **810**, 151187.

72 C. Ning, Y. Gao, H. Zhang, H. Yu, R. Cao and J. Chen, Urban particulate water-soluble organic matter in winter: Size-resolved molecular characterization, role of the S-containing compounds on haze formation, *Sci. Total Environ.*, 2023, **875**, 162657.

73 M. C. Pitts, L. R. Poole and R. Gonzalez, Polar stratospheric cloud climatology based on CALIPSO spaceborne lidar measurements from 2006 to 2017, *Atmos. Chem. Phys.*, 2018, **18**(15), 10881–10913.

74 R. D. Cook, Y. H. Lin, Z. Peng, E. Boone, R. K. Chu, J. E. Dukett, M. J. Gunsch, W. Zhang, N. Tolic, A. Laskin and K. A. Pratt, Biogenic, urban, and wildfire influences on the molecular composition of dissolved organic compounds in cloud water, *Atmos. Chem. Phys.*, 2017, **17**(24), 15167–15180.

75 S. K. Schum, B. Zhang, K. Džepina, P. Fialho, C. Mazzoleni and L. R. Mazzoleni, Molecular and physical characteristics of aerosol at a remote free troposphere site: implications for atmospheric aging, *Atmos. Chem. Phys.*, 2018, **18**(19), 14017–14036.

76 D. J. Bryant, B. S. Nelson, S. J. Swift, S. H. Budisulistiorini, W. S. Drysdale, A. R. Vaughan, M. J. Newland, J. R. Hopkins, J. M. Cash and B. Langford, Biogenic and anthropogenic sources of isoprene and monoterpenes and their secondary organic aerosol in Delhi, India, *Atmos. Chem. Phys.*, 2023, **23**(1), 61–83.

77 J. P. LeClair, J. L. Collett and L. R. Mazzoleni, Fragmentation analysis of water-soluble atmospheric organic matter using ultrahigh-resolution FT-ICR mass spectrometry, *Environ. Sci. Technol.*, 2012, **46**(8), 4312–4322.

78 J. D. Surratt, J. H. Kroll, T. E. Kleindienst, E. O. Edney, M. Claeys, A. Sorooshian, N. L. Ng, J. H. Offenberg, M. Lewandowski, M. Jaoui, R. C. Flagan and J. H. Seinfeld, Evidence for Organosulfates in Secondary Organic Aerosol, *Environ. Sci. Technol.*, 2007, **41**(2), 517–527.

79 T. Nakayama, K. Sato, M. Tsuge, T. Imamura and Y. Matsumi, Complex refractive index of secondary organic aerosol generated from isoprene/NOx photooxidation in the presence and absence of SO2, *J. Geophys. Res.: Atmos.*, 2015, **120**(15), 7777–7787.

80 W. Zhang, W. Wang, J. Li, C. Peng, K. Li, L. Zhou, B. Shi, Y. Chen, M. Liu and M. Ge, Effects of SO 2 on optical properties of secondary organic aerosol generated from photooxidation of toluene under different relative humidity conditions, *Atmos. Chem. Phys.*, 2020, **20**(7), 4477–4492.

81 T. Moise, J. M. Flores and Y. Rudich, Optical Properties of Secondary Organic Aerosols and Their Changes by Chemical Processes, *Chem. Rev.*, 2015, **115**(10), 4400–4439.

82 T. B. Nguyen, P. B. Lee, K. M. Updyke, D. L. Bones, J. Laskin, A. Laskin and S. A. Nizkorodov, Formation of nitrogen-and sulfur-containing light-absorbing compounds accelerated by evaporation of water from secondary organic aerosols, *J. Geophys. Res.: Atmos.*, 2012, **117**(D1), D01207.

83 N. E. Rothfuss and M. D. Petters, Influence of Functional Groups on the Viscosity of Organic Aerosol, *Environ. Sci. Technol.*, 2017, **51**(1), 271–279.

84 J. H. Slade, A. P. Ault, A. T. Bui, J. C. Ditto, Z. Lei, A. L. Bondy, N. E. Olson, R. D. Cook, S. J. Desrochers, R. M. Harvey, M. H. Erickson, H. W. Wallace, S. L. Alvarez, J. H. Flynn, B. E. Boor, G. A. Petrucci, D. R. Gentner, R. J. Griffin and P. B. Shepson, Bouncier Particles at Night: Biogenic Secondary Organic Aerosol Chemistry and Sulfate Drive Diel Variations in the Aerosol Phase in a Mixed Forest, *Environ. Sci. Technol.*, 2019, **53**(9), 4977–4987.

85 Y. Liu, Z. Wu, Y. Wang, Y. Xiao, F. Gu, J. Zheng, T. Tan, D. Shang, Y. Wu, L. Zeng, M. Hu, A. P. Bateman and S. T. Martin, Submicrometer Particles Are in the Liquid State during Heavy Haze Episodes in the Urban Atmosphere of Beijing, China, *Environ. Sci. Technol. Lett.*, 2017, **4**(10), 427–432.

86 J. M. Tomlin, K. A. Jankowski, F. A. Rivera-Adorno, M. Fraund, S. China, B. H. Stirm, R. Kaeser, G. S. Eakins, R. C. Moffet and P. B. Shepson, Chemical imaging of fine mode atmospheric particles collected from a research aircraft over agricultural fields, *ACS Earth Space Chem.*, 2020, **4**(11), 2171–2184.

87 J. Li, M. Pósfai, P. V. Hobbs and P. R. Buseck, Individual aerosol particles from biomass burning in southern Africa: 2, Compositions and aging of inorganic particles, *J. Geophys. Res.: Atmos.*, 2003, **108**(D13), 8484.

88 J. Liggio and S.-M. Li, Organosulfate formation during the uptake of pinonaldehyde on acidic sulfate aerosols, *Geophys. Res. Lett.*, 2006, **33**(13), L13808.

89 J. D. Surratt, Y. Gómez-González, A. W. H. Chan, R. Vermeylen, M. Shahgholi, T. E. Kleindienst, E. O. Edney, J. H. Offenberg, M. Lewandowski, M. Jaoui, W. Maenhaut, M. Claeys, R. C. Flagan and J. H. Seinfeld, Organosulfate Formation in Biogenic Secondary Organic Aerosol, *J. Phys. Chem. A*, 2008, **112**(36), 8345–8378.

90 W. Fan, T. Chen, Z. Zhu, H. Zhang, Y. Qiu and D. Yin, A review of secondary organic aerosols formation focusing

on organosulfates and organic nitrates, *J. Hazard. Mater.*, 2022, **430**, 128406.

91 S. Liu, Y. Wang, G. Wang, S. Zhang, D. Li, L. Du, C. Wu, W. Du and S. Ge, Enhancing effect of NO2 on the formation of light-absorbing secondary organic aerosols from toluene photooxidation, *Sci. Total Environ.*, 2021, **794**, 148714.

92 Q. He, S. Tomaz, C. Li, M. Zhu, D. Meidan, M. Riva, A. Laskin, S. S. Brown, C. George and X. Wang, Optical properties of secondary organic aerosol produced by nitrate radical oxidation of biogenic volatile organic compounds, *Environ. Sci. Technol.*, 2021, **55**(5), 2878–2889.

93 J. P. Reid, A. K. Bertram, D. O. Topping, A. Laskin, S. T. Martin, M. D. Petters, F. D. Pope and G. Rovelli, The viscosity of atmospherically relevant organic particles, *Nat. Commun.*, 2018, **9**(1), 956.